# Tagged Neutron Structure Function in Deuterium

A new Letter of Intent to Jefferson Lab (PAC 32)

Moskov Amarian, Stephen Bültmann (co-spokesperson), Gail Dodge, Sebastian Kuhn (co-spokesperson)*, Svyatoslav Tkachenko, Lawrence Weinstein, Jixie Zhang

*Old Dominion University*

Nathan Baillie, Keith Griffioen (co-spokesperson)

*The College of William and Mary*

Stepan Stepanyan

*Jefferson Lab*

Jerry Gilfoyle

*University of Richmond*

A CLAS collaboration Letter of Intent

* Contact: Sebastian Kuhn, Department of Physics, Old Dominion University, Norfolk VA 23529. Email: skuhn@odu.edu

**Abstract**

Twenty years after the discovery of the "EMC-effect", one of the fundamental questions at the interface of Nuclear and Particle Physics is still unanswered: How does the internal (quark–) structure of the nucleon change when the nucleon interacts with another, nearby nucleon? While many explanations and parameterizations of the EMC-effect have been proposed over the years, we don't even know for sure whether the depletion at high $x$, observed in the nuclear structure function $F_2^A(x)$, is due to a mean-field effect or due the influence of rare, but strongly modified configurations of short-range two-nucleon correlations. This is a central puzzle concerning hadron structure and interactions that needs to be solved for a full understanding of the structure of nuclear matter. Ultimately, progress on this topic can only be made when inclusive data are supplemented by high–precision semi–inclusive measurements that allow us to pin down the kinematics for each event individually.

In addition to the fundamental interest, there are also practical reasons why we need to make progress on this front. To understand the structure of the nucleon is one of the fundamental goals of nuclear and particle physics. Deep-inelastic lepton scattering off nucleon targets has produced a large amount of accurate data on the proton structure functions, but much less on those of the neutron. Because of the instability of the free neutron, its structure functions are inferred from comparative measurements between nuclear targets (e.g., deuterium) and proton targets. The precision of these measurements is limited because of the theoretical uncertainties introduced by nuclear models needed to extract information from nucleons bound in the nuclei. The BoNuS experiment (E03-012 took data at beam energies up to 5.3 GeV, and the recently approved PR12-06-113 will perform measurements at energies up to 12 GeV) will measure the neutron structure by scattering electrons off a thin deuterium gas target and detecting the low-momentum recoiling "spectator" protons in the vicinity of that target. By constraining the "spectator" proton to very low momenta and very backward scattering angles, electron scattering events on almost free neutrons can be selected. While this novel method avoids most of the nuclear binding ambiguities, it would still be helpful to study the same reaction at higher "spectator" momenta, to aid in the extrapolation to the "free neutron pole".

We propose to use the spectator technique by measuring inclusive scattered electrons in coincidence with protons of 0.2 – 0.7 GeV/c momentum, moving backward relative to the momentum transfer vector $\mathbf{q}$, in the reaction $\mathrm{D}(e, e' p_b)X$. This experiment follows the same principle as the successfully completed experiment E94-102. However, the higher beam energy of 11 GeV allows us to significantly extend the kinematic reach, covering the DIS region for a range in $x^* = Q^2/2pq$ from 0.1 to 0.6 and for "spectator" proton light cone fractions exceeding $\alpha_s = 1.4$, for a variety of transverse momenta $p_T$. CLAS12 will be used in its standard configuration, detecting electrons in the forward spectrometer with its standard set of detectors, and backward protons in the Central Tracker Silicon Vertex detectors. Assuming luminosities of $10^{35}$ $\mathrm{cm}^{-2}\mathrm{s}^{-1}$ we envision about 30 days of beam time in Hall B at 11 GeV with a liquid deuterium target (in conjunction with several other experiments planned for the deuteron).

## Collaborators' commitment to the 12 GeV upgrade of Jefferson Lab

- The Old Dominion University group (Prof. Amarian, Bültmann, Dodge, Kuhn and Weinstein) is actively involved in several other proposals using CLAS12, in addition to the present Letter of Intent. Other members of the group are pursuing 12-GeV proposals for Hall A, but their contributions are not included here. In support of our strong interest in Physics with CLAS12, our group has taken on responsibility for a major component of the CLAS12 baseline equipment. The group has begun work on the design and prototyping of the new Region I drift chambers for CLAS12. This work has involved the faculty, two graduate students, several undergraduate students and a technician. We have set up a data acquisition system to test various prototype chambers and have been involved and the detailed engineering design of the chamber, parts of which have already entered the procurement phase.

  As a result of an in-depth review of the whole CLAS12 tracking project (of which one of us is a co-organizer), it was decided that our group will ultimately design, prototype, construct and test the Region 2 Drift Chambers. A Memorandum of Understanding between ODU and JLab to this end has been executed. We expect to continue our strong commitment of manpower to this project. Funding for the group is from DOE and from the university (75% of research faculty salary + one regular faculty summer salary + 50% of the technician). The university has also provided 6000 square feet of high bay laboratory space with clean room capabilities for our use. We will seek other sources of funding as appropriate. Gail Dodge is the chair of the CLAS12 Steering Committee and the user coordinator for the CLAS12 tracking technical working group. Sebastian Kuhn is the user coordinator for beamline elements. Beyond the baseline equipment, the group is also interested in working on improvements to the existing BoNuS detector.

- The College of William and Mary group is actively involved in this proposal, as well as several other proposals using CLAS12. Other members of the group are also pursuing a proposal for Hall A, but their contributions are not included here. Among CLAS12 baseline equipment, the group is committed to building part of the forward tracking system, but the exact tasks have not yet been determined. At least one faculty member, two graduate students, half a post-doc and several undergraduates are likely to work at least part time on this project in the next few years. Funding for the group is from the DOE and from the NSF. Additional funding will be sought for building the base equipment. Facilities at William and Mary include a clean room suitable for drift-chamber construction, and, on the time scale of a few years in the future, ample space for detector construction and testing.

# Contents

**1 Introduction** **4**
1.1 Existing Data from E94-102 . . . . . 5

**2 Theoretical Background** **7**
2.1 Spectator tagging . . . . . 7
2.2 Modifications of the simple spectator picture . . . . . 8
2.2.1 Target fragmentation . . . . . 9
2.2.2 Off-shell effects . . . . . 9
2.2.3 Final state interactions . . . . . 14

**3 Experimental Details** **17**
3.1 Deuterium Target . . . . . 17
3.2 Central Detector Solenoid . . . . . 19
3.3 Central Detector . . . . . 19

**4 Expected Results** **21**

**5 Summary** **25**

# 1 Introduction

For a complete understanding of QCD at hadronic scales, we need to learn more about the interplay between the internal (quark) structure of nucleons and the interaction between two nucleons. In particular, it is of high interest whether nucleons in close proximity to each other change their internal structure or may even lose their separate identity to fuse into a "six quark cluster" [1]. Some less dramatic modifications of the nucleon structure that have been proposed include off-shell effects [2], $Q^2$ rescaling effects [3] and the suppression of small-size configurations (PLCs) in the nucleon wave function [4, 5]. In a recent review [6], it was pointed out that by studying nucleons at short inter-nucleon distance, one can shed light on a so-far unexplored part of the QCD phase diagram, the region of high baryon density and low temperature where novel effects like color superconductivity might be expected.

The most famous consequence of possible modifications of the nucleon structure inside nuclei is the observation by the EMC collaboration [7] that the deep inelastic (DIS) structure function $F_2^A(x)$ of a nucleus differs non-trivially from the sum of free nucleon structure functions $F_2^p(x)$, $F_2^n(x)$. A large number of theoretical explanations of this effect have been brought forward; for a recent attempt to provide a unified description of the large set of experimental data see Ref. [8]. However, inclusive measurements cannot distinguish unambiguously between these different approaches, since they integrate over all possible momenta of the struck nucleons. Therefore, it remains an open and very interesting question whether the "EMC-effect" is just a mean-field influence on the average bound nucleon, or whether there is a particular strong contribution from nucleons that are moving with momenta significantly above the Fermi edge. Progress requires more detailed, semi-inclusive studies, where additional information about the kinematics of each event can be inferred. Some first results obtained using this approach have been extracted [9] from existing Fermilab [10] and CERN [11] data where neutrino scattering on deuterium and heavier nuclei was observed in coincidence with backward-going protons. While these data show some interesting results, the available statistics and resolution are too limited for the necessary fine binning in all kinematic variables. More recently, an experiment at Jefferson Lab (94-102) measured 5.75 GeV electrons scattering off deuterium with the simultaneous detection of 0.3 – 0.7 GeV/c protons moving backwards relative to the momentum transfer direction [12]. This experiment is summarized in more detail below.

Apart from the intrinsic interest, we must gain a better understanding of how the cross-section of electron-bound neutron scattering (e.g., from scattering on deuterium) is modified in comparison to the electron-free neutron one if we are to improve our knowledge of neutron structure. In the absence of free neutron targets, all our information on the neutron has been obtained from scattering off nuclear targets. Unfortunately, the binding and off-shell effects on measurements of neutron properties can be large and unknown, especially at kinematics that emphasize the higher-momentum components of the nuclear wave function (e.g., low $W$ and high $x$). A new experimental program at Jefferson Lab is devoted to the extraction of neutron structure information from electron scattering measurements on deuterium, by simultaneously detecting low-momentum (less than 0.1 GeV/c) "spectator" protons scattered in the backward direction. The "BoNuS" experiment (E03-012) has already taken data with CLAS with beam energy ranging from 1.1 to 5.3 GeV and is presently under analysis; the "BoNuS12" utilizing the energy-upgraded JLab and CLAS12 (PR12-06-113 [13]) has been

approved (conditionally) by PAC30. While the choice of kinematics for "BoNuS" strongly reduces nuclear effects, it would substantially reduce our remaining systematic error if we could also measure the same reaction at larger proton momenta, to study deviations from the spectator picture and put the extrapolation towards the "free neutron pole" on firm footing. In general, once we understand the origin of the EMC effect and the role of tightly correlated nucleon pairs, we can use the vast existing data set from higher-energy labs like SLAC to extract information on the neutron with more confidence.

Deuterium is the optimal system to study such "tightly bound pairs", since there are no additional nucleons interacting with the pair under study and the pair is at rest in the lab frame, its kinematics being completely defined. While the probability for a small internucleon distance configuration in deuterium is rather small compared to heavier nuclei, such configurations can be "tagged" by the emission of a fast proton in the backward hemisphere relative to the momentum transfer vector. We therefore propose to measure the reaction $D(e, e'p_b)X$ with coincident detection of the scattered electron in the forward part of the CLAS12 and the fast (0.2–0.7 GeV/c) proton in the central detector.

In a simple spectator picture, the backwards moving proton does not participate in the scattering process and can serve as a tag of the initial state momenta of both nucleons. By measuring the momentum of this backward proton, we can correct the observed electron kinematics for the initial motion of the unobserved struck neutron and extract the modified neutron structure function $F_2^{n(eff)}(x, Q^2, p^2)$. This technique is very similar to that envisioned in the BoNuS12 proposal [13] but the emphasis here is not on nearly on–shell neutrons, but rather on the opposite kinematic extreme of fast–moving neutrons ($p^2 << M^2$) where off-shell effects and other internal structure changes are much more pronounced.

## 1.1 Existing Data from E94-102

We conclude this introduction with a brief summary of the results from E94-102, which can be considered the precursor experiment to the one proposed here. E94-102 took place in spring of 2002. It used a 5.75 GeV electron beam impinging on a 5 cm long liquid deuterium target, yielding a luminosity of $10^{34}\mathrm{cm}^{-2}\mathrm{s}^{-1}$. Both scattered electrons and "spectator" protons were detected with the standard CLAS detector elements. While the experiment covered a relatively large range in spectator light-cone fraction $\alpha_s$ and $x^*$ (kinematically corrected Bjorken $x$), most of the kinematics was for rather large transverse momenta, $p_T > 0.3$ GeV/c and below the limit of the DIS region, $W^* < 2$ GeV. (For a definition of all the variables introduced here see the next section). As a consequence, we found that final state interaction (FSI) effects were rather important for much of the kinematics covered, so that an unambiguous extraction of neutron structure modifications from this experiment wasn't possible. However, our data give us a valuable guidance towards an optimization of the 11 GeV extension proposed here.

The following figures summarize some of our findings. Figure 1 shows that the PWIA spectator picture describes our data rather well for proton angles larger than 107 degrees relative to the momentum transfer direction (panel a). On the other hand, at angles around 90 degrees (panel b), a large excess of high-momentum protons over the PWIA spectator expectation is observed, which is most likely due to strong final state interactions. Both the kinematic dependence and the magnitude of this excess are in rather good agreement with

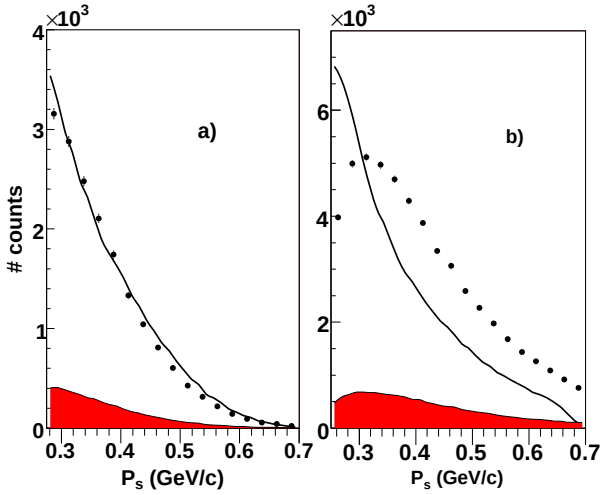


Figure 1: Momentum distribution of the recoiling proton. Data (points) are compared with our MC simulation (solid curve) for the range of recoil angle $-1.0 < \cos\theta_{pq} < -0.3$ (a) and $-0.3 < \cos\theta_{pq} < 0.3$ (b). Events were integrated over all missing masses and $Q^2$.

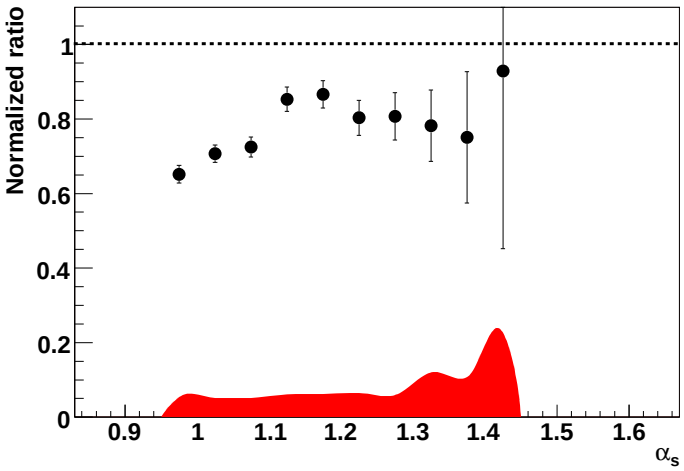


Figure 2: Ratio of the extracted "off-shell" structure function $F_{2n}$ at $x^* = 0.55, Q^2 = 2.8$ (GeV/c)$^2$ to that at $x = 0.25, Q^2 = 1.8$ (GeV/c)$^2$, divided by the ratio of the free structure functions at these kinematic points. The error bars are statistical only and the shaded band indicates the overall systematic error. This plot is for similar (but not identical) kinematics as Fig. 6 in the paper by Melnitchouk *et al.* [15].

recent calculations [14] of these FSI effects for the reaction studied here.

Figure 2 shows the $\alpha_s$-dependence of the ratio of extracted "off-shell" neutron structure functions $F_{2n}$ at high $x^* = 0.55$ (where the EMC effect should be largest) to $F_{2n}$ at low $x^* = 0.25$ (where the EMC effect is less prominent), normalized to the same ratio for the

free neutron structure function. While the data seem to indicate a suppression of $F_{2n}$ at high $x^*$, our kinematics are at the transverse momentum of $p_T = 0.3$ GeV/c where FSI effects may play a big role, especially around $\alpha_s \approx 1$. All theoretical models (for $p_T = 0$) predict unity for $\alpha_s \approx 1$ and a fall-off for higher values of $\alpha_s$ (see the following section). To fully explore these predictions, a substantially higher beam energy is needed to simultaneously access the DIS region and larger backward angles.

# 2 Theoretical Background

## 2.1 Spectator tagging

The measurement of tagged structure functions in semi-inclusive deep inelastic scattering (DIS) from the deuteron with a slow recoil proton detected in the backward hemisphere, $e + D \rightarrow e + p + X$, can be described in the nuclear impulse approximation, in which the inelastic scattering takes place incoherently from individual nucleons. In this picture, the differential semi-inclusive cross section can be written as a product of the deuteron spectral function, $\mathcal{S}$, and an effective (bound) neutron structure function, $F_2^{n(eff)}$ [15]:

$$\frac{d\sigma}{dx dW^2 d\alpha_s d^2p_T} \approx \frac{2\alpha_{em}^2(1-\nu/E)}{Q^4}\ \alpha_s\ \mathcal{S}(\alpha_s, p_T)\ F_2^{n(eff)}(W^{*2}, p^2, Q^2)\ . \tag{1}$$

(For the full expression for the differential cross section in terms of the transverse and longitudinal structure functions see Ref. [15].) Here $W^{*2} = (p_d + q - p_s)^2$ is the invariant mass squared of the unobserved hadronic final state, with $p_s$ the momentum of the spectator proton, $p_d$ the momentum of the initial state deuteron, and $p = p_d - p_s$ the momentum of the struck neutron. The variable $\alpha_s = (E_s - p_s^z)/M$ is the light-cone momentum fraction carried by the spectator proton, and $p_T$ its transverse momentum component (perpendicular to the direction of $\vec{q}$), with $E_s = \sqrt{M^2 + \vec{p}_s^{\,2}}$ the spectator proton energy, and $M$ its mass. Instead of the invariant mass $W^*$ one can also use the kinematically corrected nucleon momentum fraction $x^* = Q^2/2q(p_d - p_s)$ as one of the independent variables for $F_2^{n(eff)}$. The use of the light-cone variable $\alpha_s$ emphasizes the kinematical dependence of the structure function at high $Q^2$, since in that limit $x^* \approx x/(2-\alpha_s)$, with $x = Q^2/2M\nu$ the ordinary definition of the Bjorken scaling variable. In addition, as discussed in Section 2.2.3 below, the dependence on $\alpha_s$ is not affected by final state interactions. The pre-factor $\alpha_s$ in Eq. (1) is related to the so-called "flux-factor" [16]. The degree to which the struck neutron is off-shell is given by

$$M^2 - p^2 \approx 2\vec{p}_s^{\,2} + 2M|\epsilon|\ , \tag{2}$$

where $\epsilon$ is the deuteron binding energy. In the limit $p^2 \rightarrow M^2$ (and $\alpha \rightarrow 1$), the effective neutron structure function $F_2^{n(eff)}(W^2, Q^2, p^2) \rightarrow F_2^n(W^2, Q^2, M^2) \equiv F_2^n(x, Q^2)$, the free neutron structure function. The $p^2$ dependence of $F_2^{n(eff)}$ depends on the theoretical assumptions made about the off-shell behavior of the photon–bound nucleon scattering amplitude, and includes possible structure modifications of neutrons during short-distance fluctuations of the proton-neutron system.

To extract the free neutron structure, one therefore needs to minimize the degree to which the struck neutron is off-shell, by restricting oneself to small values of the spectator proton

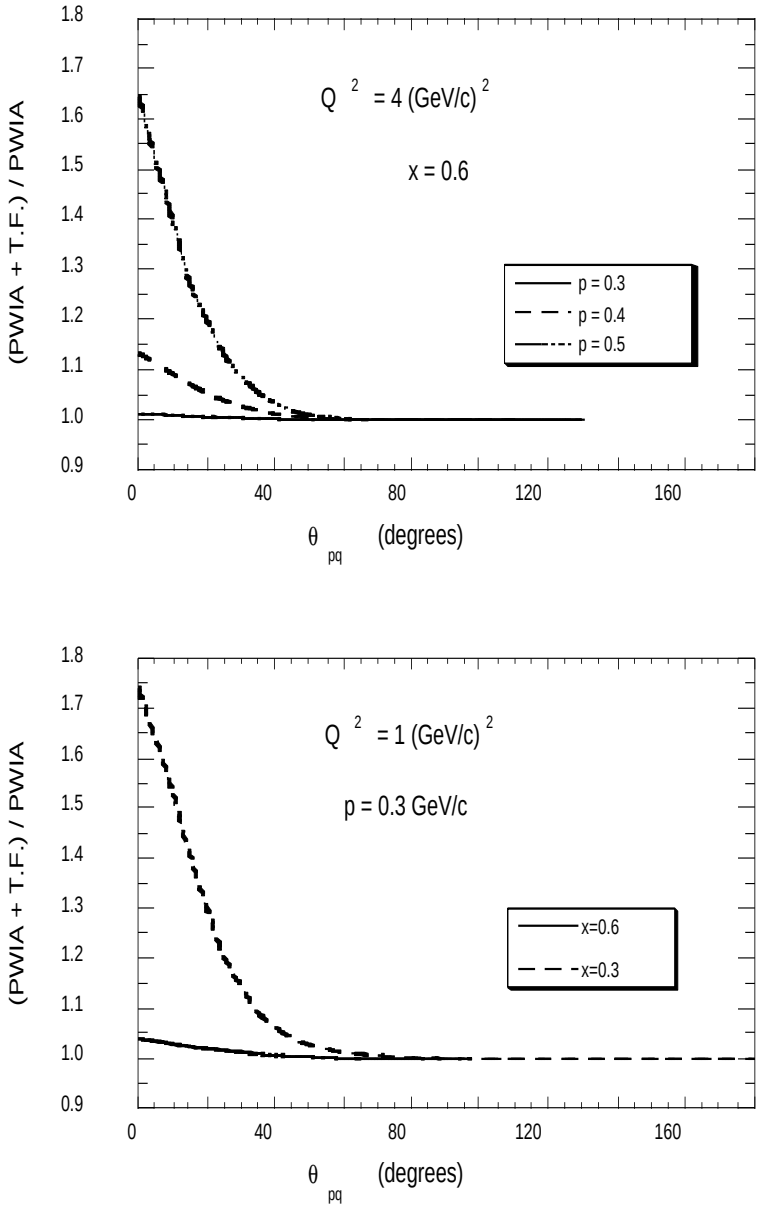


Figure 3: Effect of target fragmentation (TF) on the plane wave impulse approximation (PWIA) calculation of semi-inclusive DIS from the deuteron [18], as a function of the c.m. angle, $\theta_{pq}$, between the spectator proton and the virtual photon.

momentum, $p_s$. Conversely, to study the behavior of far off-shell nucleons and to test various models of the EMC-effect, one should select large spectator momenta (or, equivalently, large $\alpha_s$).

## 2.2 Modifications of the simple spectator picture

In this section we consider several corrections to the impulse approximation in Eq. (1) explicitly. Corrections to the impulse approximation from the breaking of the factorization in

Eq. (1) were analyzed in Ref. [17] for the inclusive deuteron structure function, and found to be quite small ($\leq 1\%$) for the kinematics considered here.

### 2.2.1 Target fragmentation

The production of low momentum protons originating from the hadronic debris of the struck neutron is minimized by enforcing a large rapidity gap between the recoil proton and the rest of the hadronic debris [18, 19]. While in the forward hemisphere (current fragmentation region) there are potentially large contributions from direct quark→proton fragmentation, especially at low $x$, in the backward hemisphere (target fragmentation) these will be strongly suppressed. The direct fragmentation contribution is also expected to decrease with decreasing spectator proton momentum.

These features are evident from Fig. 3, where the ratio of the plane wave impulse approximation (PWIA), corrected for target fragmentation, to the pure PWIA contribution is shown as a function of the recoil angle, $\theta_{pq}$, of the proton relative to the photon direction. Clearly, the effects of target fragmentation are relevant only in the forward hemisphere, and for $\theta_{pq} > 90^\circ$ are totally negligible, even for large $p_s$. An estimate of the importance of target fragmentation can also be made by measuring the rate of backward protons produced from a hydrogen target, which can then be used to calibrate this contribution.

### 2.2.2 Off-shell effects

In convolution models off-shell corrections appearing at leading twist originate both kinematically, as a consequence of the nucleon's transverse motion in the nucleus, and dynamically, from modifications of the bound nucleon structure. Kinematical off-shell effects can be calculated with very little model dependence, as discussed in Ref. [20], for instance. Dynamical off-shell effects, on the other hand, depend on descriptions of the intrinsic deformation of the bound nucleon structure, and are therefore more model-dependent.

In the covariant spectator model of Ref. [17], the DIS from a bound nucleon is described in terms of relativistic vertex functions which parameterize the nucleon–quark–"diquark" interaction (where "diquark" here refers to a system of a nucleon with one quark removed, which has the quantum numbers of a diquark). The dependence of the vertex functions on the quark momentum and the "diquark" energy is constrained by fitting to the on-shell nucleon (proton) structure function data. The additional dependence of the vertex function on the virtuality of the off-shell neutron is fixed by comparing the calculated deuteron structure function with the inclusive $F_2^d$ data. The resulting ratio $R_n \equiv F_2^{n(eff)}(W^2, Q^2, p^2)/F_2^n(W^2, Q^2)$ of the bound to free neutron structure functions is shown in Fig. 4 as a function of the momentum of the spectator proton, $|\vec{p}_s| = |\vec{p}|$, for several values of $x$. Not surprisingly, the effect at low $|\vec{p}_s|$ is very small, with the deviation from unity increasing at higher momenta. For $|\vec{p}| \approx 100$ MeV/c the effect is $\leq 1\%$ for $x = 0.6$, where the EMC effect is more pronounced, and essentially zero for $x = 0.3$. Even at higher momenta, this approach yields a rather moderate modification of the nucleon structure function inside a nucleus.

A similar model in which the scattering from an off-shell nucleon is described in terms of a relativistic quark spectral function was introduced in Ref. [20]. In this approach the bound nucleon structure function is evaluated from the free nucleon structure function at a

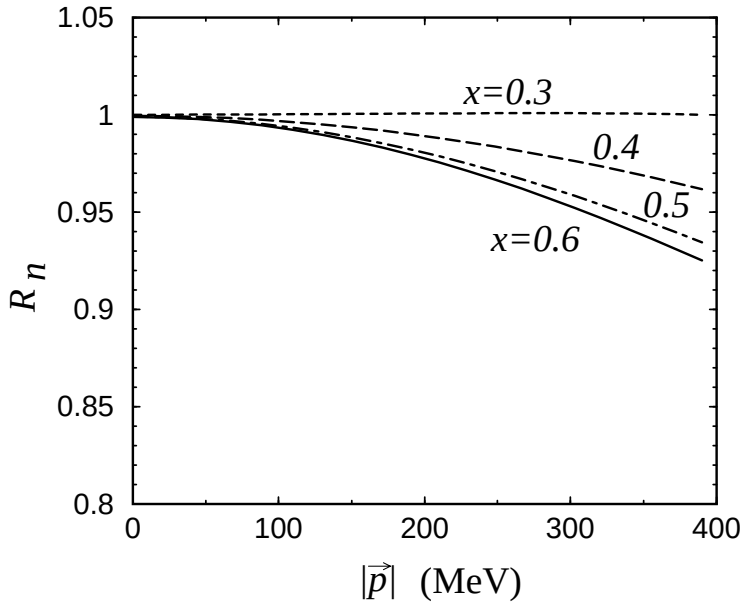


Figure 4: Ratio $R_n \equiv F_2^{n(eff)}(W^2, Q^2, p^2)/F_2^n(W^2, Q^2)$ of the bound to free neutron structure functions, as a function of the spectator proton momentum, in the model of Ref. [17], at $Q^2 = 5$ (GeV/$c$)$^2$.

shifted value of the quark light-cone momentum fraction, which depends on the mass of the spectator "diquark" system, the bound nucleon momentum, and the binding energy [20]. The resulting ratio $R_n$ of the bound to free neutron structure functions is shown in Fig. 5.

The deviation from unity is again small at low spectator proton momenta, amounting to $\leq 2\%$ for $|\vec{p}_s| \leq 100$ MeV/c, increasing to around 5% for $|\vec{p}_s| = 200$ MeV/$c$. However, the off-shell effects in this model increase more rapidly as the spectator momentum increases. The results shown are for $Q^2 = 10$ (GeV/$c$)$^2$, although the $Q^2$ dependence is weak. In contrast to Fig. 4, the effect in this model is only weakly dependent on $x$. Similar behavior to that in Figs. 4 and 5 is also observed in the model of Ref. [21], where the assumption of weak binding in the deuteron allows one to calculate the off-shell dependence up to order $p^2/M^2$. An important constraint on the size of the nucleon's deformation in this approach is provided by the conservation of the number of valence quarks in the bound nucleon,

$$\frac{d}{dp^2} \int_0^1 dx \, q_{val}^{(eff)}(x, Q^2, p^2) = 0 \ , \tag{3}$$

where $q_{val}^{(eff)}$ is the valence quark distribution in the effective nucleon structure function, $F_2^{N(eff)}$. By imposing this constraint, one obtains an overall reduction of the kinematical off-shell effects whose strength can be located either at intermediate values of $x$, $x \geq 0.4$, as in the models of Refs. [17, 21], or at low values of $x$, $x \leq 0.15$, as suggested in Ref. [22].

Neglecting the contributions of $N\bar{N}$ pairs to the deuteron wave function, another estimate of the role of nucleon off-shellness can be made simply on the basis of kinematics. In the instant form approach discussed in Ref. [23], the nuclear structure function is related to the free nucleon structure function, evaluated at a shifted energy transfer, $\nu \to \bar{\nu}$, which depends on the degree to which the nucleon is bound (and hence, in the instant form language, off its

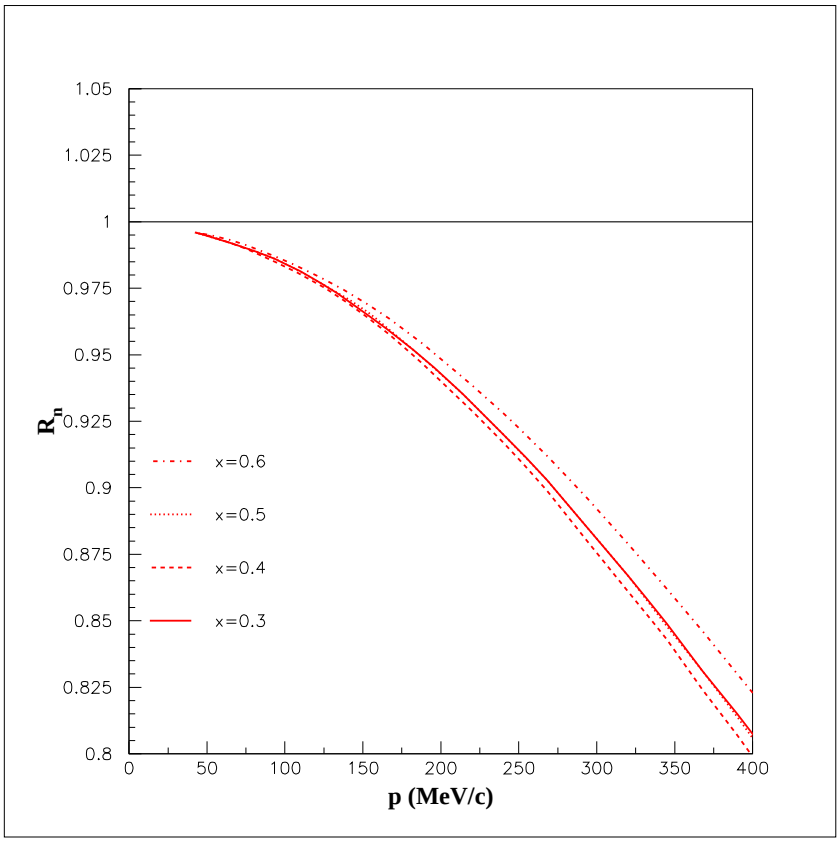


Figure 5: Ratio $R_n$ of the bound to free neutron structure functions, as a function of the spectator proton momentum, in the model of Ref. [20].

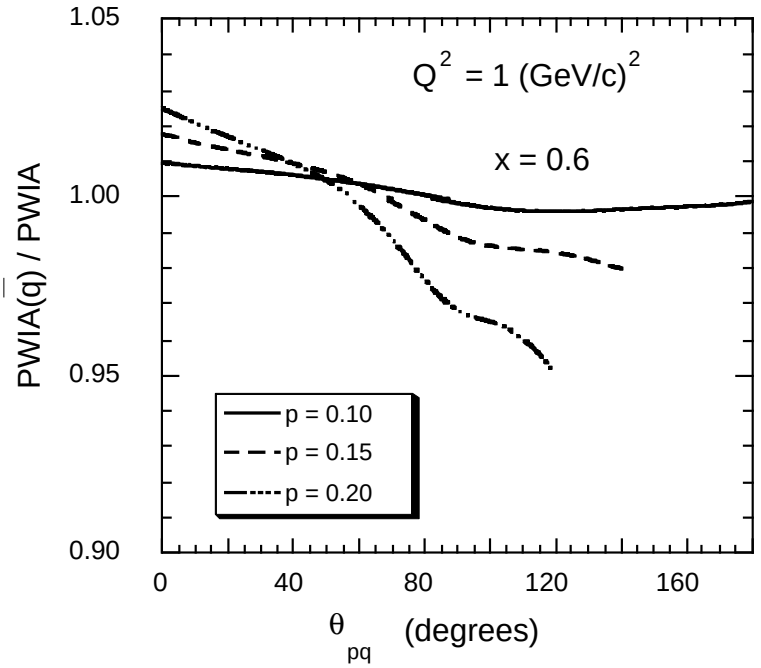


Figure 6: Ratio of bound to free nucleon structure functions, calculated using the model of Ref. [23]. The spectator proton momentum $p$ is in units of GeV/$c$.

energy shell). A shifted value of $\nu$ corresponds to a shifted value of $x$ and $Q^2$ at which the nucleon structure function is evaluated. The ratio of the structure functions calculated in the plane wave impulse approximation with the modified variables ("PWIA($\bar{q}$)") to that in which there is no modification is displayed in Fig. 6 as a function of $\theta_{pq}$ for $Q^2 = 1$ (GeV/$c$)$^2$. Once again, one sees that for low spectator proton momenta, $|\vec{p}_s| \approx 100$ MeV/$c$, the off-shell modification is less than 1% for all accessible angles. Only when one goes above $|\vec{p}_s| \approx 200$ MeV/$c$ are there any effects at the $\leq 5\%$ level.

While the off-shell modification of the bound nucleon structure function in the above models is weak, the color screening model for the suppression of point-like configurations in bound nucleons [5] predicts significantly larger deviations from unity of the ratio $R_n$ than that in Figs. 4, 5 and 6. In this model one attributes most or all of the EMC effect to a medium modification of the internal structure of the bound nucleon, and little of the effect to mechanisms such as nuclear binding. This leads to a much stronger dependence of the off-shell neutron structure function on $p_s$ or $\alpha_s$, especially at high $x^*$.

This last prediction (with the strongest off-shell dependence), together with the first one (least dramatic off-shell effects) and an intermediate model proposed to explain the EMC effect by Close et al. [3], is shown in Fig. 7. (The figure is taken from Ref. [15] and should be compared to the results from E94-102 in Fig. 2.) As can be seen, the three representative models all predict small off-shell effects around $\alpha_s \approx 1$ which corresponds to small spectator momentum. However, they differ dramatically from each other at higher values of $\alpha_s$, as much as a 33% already at $\alpha_s = 1.4$. Our goal for the proposed experiment is therefore to cover the range $\alpha_s = 1...1.4$ and simultaneously $x^* = 0.2...0.6$ to directly test the predictions shown in Fig. 7. For this, it is also important to stay within the DIS region ($W^* > 2$

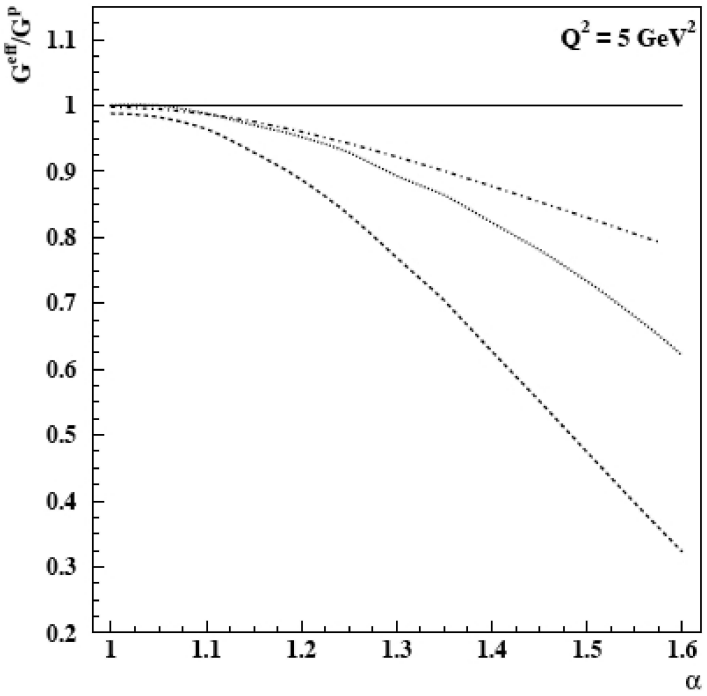


Figure 7: Comparison of the expected dependence of the ratio of the off-shell structure function $F_2^{n(eff)}$ at $x^* = 0.6$ to that at $x^* = 0.2$ on the light cone fraction $\alpha_s$, according to 3 different models (see text for details). The curves are normalized to the free ratio.

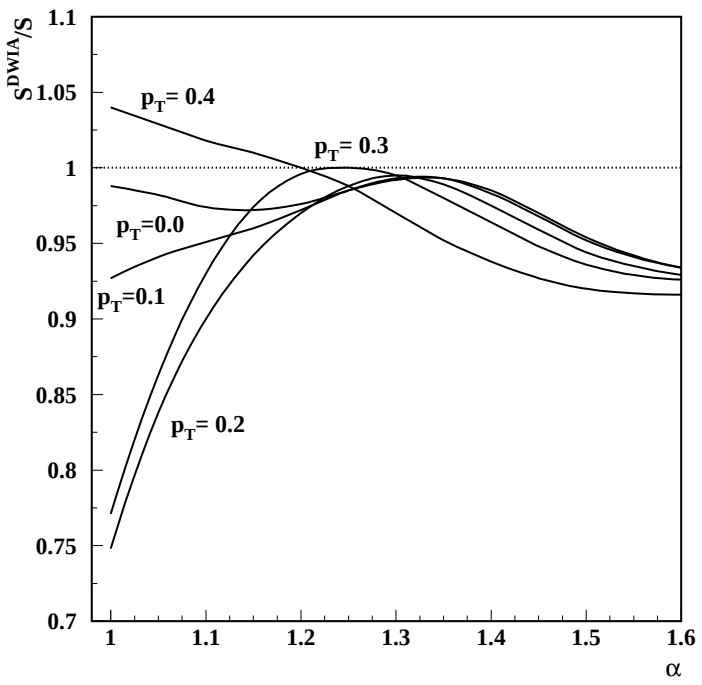


Figure 8: Spectral function calculated with and without FSI effects within the DWIA [15]. The curves correspond to different values of the spectator proton transverse momentum $p_T$ (in GeV/$c$).

GeV) and at the smallest possible transverse momenta $p_T$ (all curves in the figure assume $p_T = 0$). This combination of kinematic requirements can only be fulfilled at the highest energy available at the upgraded CEBAF, 11 GeV.

An even more dramatically different dependence of the structure function ratio on $\alpha_s$ and $x^*$ is predicted by the model of Carlson et al. [1]. In this model, a part of the deuteron wave function consists out of fully kneaded 6-quark states, and instead of the spectator mechanism, Eq. 1, one has to consider the momentum distribution of quarks inside this "6-quark bag" combined with the fragmentation function describing the emergence of a backward proton in the final state.

### 2.2.3 Final state interactions

The simple spectator picture described so far has to be modified to account for final state interaction (FSI) effects, or rescattering of the spectator proton by the deep inelastic remnants, $X$, of the scattered neutron. The choice of backward angles is designed to minimize these effects. The magnitude of FSI effects has been estimated in several models, within the framework of the distorted wave impulse approximation (DWIA) [24], and in a string-like model which emphasizes the propagation and hadronization of the partonic debris emanating from the photon–bound nucleon vertex [14]. The strong suppression of FSIs at backward spectator proton angles is evident in both of these calculations.

A direct calculation of the FSI contribution to the cross section requires knowledge of the full dynamics of the spectator proton–$X$ system. In the model of Ref. [24] the effects of FSIs are estimated by comparing with the calculation of FSI effects in the high-energy $^2$H$(e,e'p)n$ break-up reaction. The effective $p$–$X$ interaction cross section, $\sigma_{eff}$, is approximated [25] by that extracted from soft neutron production in the high-energy DIS of muons from heavy nuclei [26]. The effect of the FSI is then to modify the spectral function $\mathcal{S} \to \mathcal{S}^{DWIA}$ [24], where

$$\mathcal{S}^{DWIA}(\alpha, p_T \approx 0) \sim \mathcal{S}(\alpha, p_T \approx 0) \left[ 1 - \frac{\sigma_{eff}(Q^2,x)}{8\pi \langle r^2_{pn} \rangle} \frac{|\psi_d(\alpha, \langle p_T \rangle) \psi_d(\alpha, 0)|}{S(\alpha, p_T \approx 0)/\sqrt{E_s \; E_s(\langle p_T^2 \rangle)}} \right] , \quad (4)$$

with $\langle r^2_{pn} \rangle$ the average separation of the nucleons within the deuteron, and $E_s(\langle p_T^2 \rangle) = \sqrt{M^2 + {p_s^z}^2 + \langle p_T^2 \rangle}$ the energy evaluated at the average transverse momentum, $\langle p_T^2 \rangle^{1/2} \sim$ 200–300 MeV/$c$, transferred for the hadronic soft interactions with effective cross section $\sigma_{eff}$. The steep momentum dependence of the deuteron wave function, $|\psi_d(\alpha, \langle p_T \rangle)| \ll |\psi_d(\alpha, p_T \approx 0)|$, ensures that FSI effects are suppressed in the extreme backward kinematics.

The effects of FSIs in this model are illustrated in Fig.8, which shows the ratio of the light-cone spectral function including FSI effects within the DWIA to that without [15]. At extreme backward kinematics ($p_T \approx 0$) one sees that FSI effects contribute less than $\sim 5\%$ to the overall uncertainty of the $d(e,e'n)X$ cross section for $\alpha_s \leq 1.5$. For $p_T = 0.1$ GeV/$c$ the FSI effects are minimized at $\alpha_s = 1.3$, and remain at the $\leq 8\%$ level for values of $\alpha_s$ ($\alpha_s = 1...1.4$) typical for the proposed experiment.

A more microscopic treatment of the effective rescattering cross section was developed recently in Ref. [14]. Here the FSI due to the propagation of the struck nucleon debris and its hadronization in the nuclear environment was applied to the $A(e,e'(A-1))X$ reaction, in which the residual $(A-1)$ nucleus is detected in coincidence with the scattered lepton. For a deuteron target, this process precisely coincides with that considered here, namely $^2$H$(e,e'N)X$. The effective cross section, $\sigma_{eff}$, describing the interaction of the debris with a nucleon of the $(A-1)$ spectator system in this approach is both time ($t$) and $Q^2$ dependent. This result was obtained on the basis of a model [14] which takes into account both the production of hadrons due to the breaking of the color string, which is formed after a quark is knocked out from a bound nucleon, as well as the production of hadrons originating from gluon radiation [27]. The general expression has the form:

$$\sigma_{eff}(t) = \sigma_{tot}^{NN} + \sigma_{tot}^{\pi N} \Big[ n_M(t) + n_G(t) \Big] , \quad (5)$$

where $\sigma_{tot}^{NN}$ and $\sigma_{tot}^{\pi N}$ are the total nucleon-nucleon and meson-nucleon scattering cross sections, and $n_M(t)$ and $n_G(t)$ are the effective numbers of created mesons and radiated gluons, respectively. The dependence of $\sigma_{eff}$ on $t$ (or equivalently on $z$, the longitudinal distance) and $Q^2$ or $W$ is illustrated in Fig. 9.

Once the effective cross section of the interaction of the quark debris with the nucleons is defined, the standard eikonal approximation can be used to evaluate the cross section by replacing the struck nucleon momentum distribution with the distorted momentum distribution [28],

$$S^{PWIA}(\vec{p}_s) \to S^{FSI}(\vec{p}_s) = \frac{1}{3} \frac{1}{(2\pi)3} \sum_{\mathcal{M}_d} \left| \int d\vec{r} \; \Psi_{1,\mathcal{M}_d}(\vec{r}) S(\vec{r}) \chi_f^\dagger \exp(-i\vec{p}_s \cdot \vec{r}) \right|^2 , \quad (6)$$

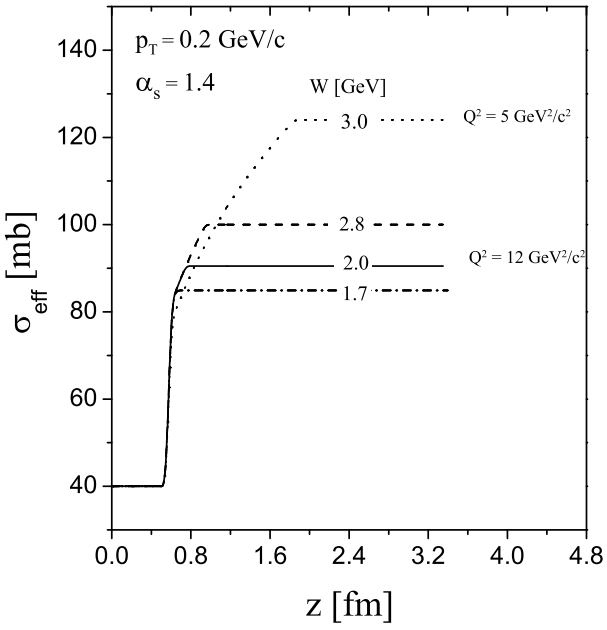


Figure 9: The debris–nucleon effective cross section, $\sigma_{eff}$, from Eq. (5) [14], as a function of the longitudinal distance $z$.

where the relative coordinate $\vec{r} = \vec{b} + z\vec{q}/|\vec{q}|$ is defined in terms of the longitudinal, $z$, and perpendicular, $\vec{b}$, components, with the $z$ axis along $\vec{q}$. Here $\chi_f$ is the spin wave function of the final state, and $S(\vec{r})$ is the $S$-matrix describing the final state interaction between the debris and spectator nucleon,

$$S(\vec{r}) = 1 - \theta(z)\,\frac{\sigma_{eff}(z)(1-i\beta)}{4\pi b_0 2}\,\exp(-b^2/2b_0^2)\ , \tag{7}$$

where $\beta$ is the ratio of the real to imaginary parts of the scattering amplitude, and the step function $\theta(z)$ arises from the high energy approximation of the Glauber theory. The above equations can also be used to calculate quasi-elastic scattering by replacing the debris-nucleon cross section with the nucleon-nucleon cross section.

The effects of FSIs in this model are illustrated in Fig. 10, where the ratio of spectral functions with and without FSI corrections is shown as a function of $\theta$ and $|\vec{p}_s|$. For low spectator momenta, $|\vec{p}_s| \leq 100$ MeV/$c$, the effects at backward angles ($\theta \geq 130^\circ$) are quite small, $\leq 5\%$. At larger momenta, $|\vec{p}_s| \approx 200$ MeV/$c$, FSIs introduce some 20–30% enhancement of the spectral function. The effects of FSIs become dominant at perpendicular angles, $\theta \sim 90^\circ$, where for $|\vec{p}_s| = 200$ MeV/$c$ they reduce the ratio of spectral functions by some 75%. Of course, the study of FSI and hadronization effects is interesting in its own right, and can be pursued by focusing on the kinematical region around $\theta \sim 90^\circ$. On the other hand, the results of the model calculations in Figs. 8 and 10 give us confidence that the

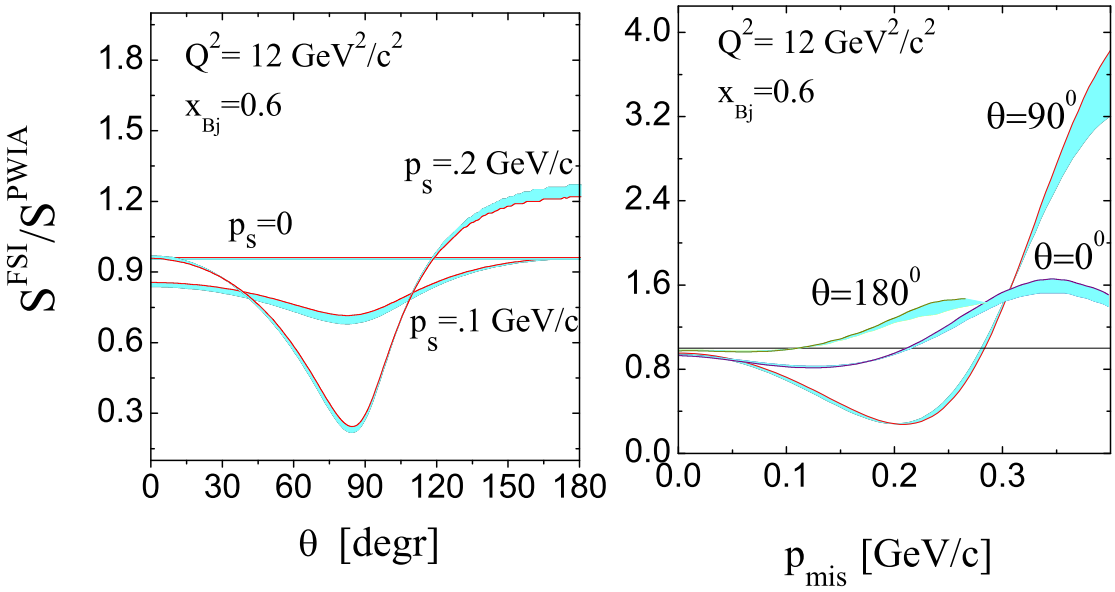


Figure 10: The momentum and angular dependence of the ratio $S^{FSI}/S^{PWIA}$, at $Q^2$ = 12 GeV$^2/c^2$ and $x = 0.6$ (updated calculations by the authors of [29]). Left panel: dependence on the angle between the spectator proton and the virtual photon direction. Right panel: dependence on spectator momentum.

effects of FSIs at backward angles are relatively small. Clearly, all models indicate that to minimize FSI, one has to minimize $p_T$ while varying $\alpha_s$. This is already born out by the existing E94-102 data, see the Introduction. At the higher beam energy available with the upgraded CEBAF, we will be able to compare the $\alpha_s$ dependence of any off-shell effects for several different fixed $p_T$, which should allow us to test and fine-tune models of FSI and to extrapolate to the simple, FSI-free spectator picture.

# 3 Experimental Details

The Deeps12 experiment will use the CLAS12 forward detector together with the central detector, which will be used for the detection of the recoiling spectator protons through the silicon vertex tracker (SVT) and the central time of flight detector (CToF). The target inside the central detector will be a five centimeter long liquid deuterium cell.

## 3.1 Deuterium Target

The cryogenic liquid deuterium target will be 5 cm long. It will be similar to the one used by the Deeps experiment E94-102.

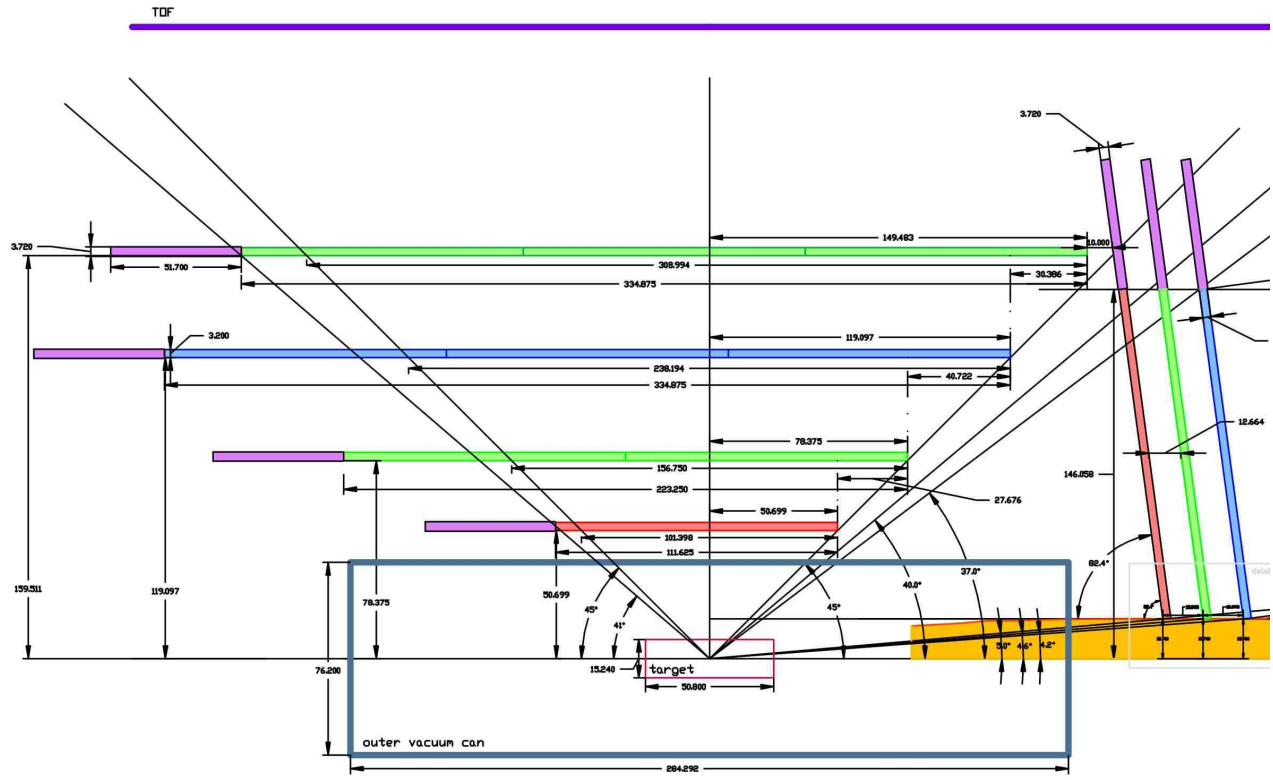


Figure 11: Present schematic design of the silicon vertex tracker (detailed view). In this view, the target is 5 cm long and centered inside the solenoid. The red, green, and blue panels represent the silicon double layers.

## 3.2 Central Detector Solenoid

Both the target and the central detector will be located inside the central detector solenoidal magnet. The longitudinal magnetic field from this solenoid forces the Møller electrons onto helical trajectories into the forward direction along the beam axis, hence, suppressing this background. The solenoid will also provide the analyzing magnetic field for bending the recoil proton tracks inside the SVT for the momentum measurement.

## 3.3 Central Detector

A design schematic of the central detector, featuring the silicon vertex tracker and central time of flight detector, is shown in Fig. 11.

The target is shown in the *standard* center position inside the solenoid. In this location, the scattering angle is limited to values between 45° and 139° (most backward) for the central target point. However, the CToF scintillation counter is covering only a smaller range.

Since the spectator protons of interest are scattered at large backward angles, moving the target cell forward along the beamline will increase the backward angle coverage. A downstream shift of the target by eight centimeters will increase backward angles coverage to almost 160° at an average momentum of 270 MeV/$c$, while loosing some forward coverage.

A simulation has been set up that uses the CLAS12 detector FastMC. To integrate energy loss of the scattered low momentum spectator protons, the central detector has been modeled by an independent simulation. This central detector simulation includes the liquid deuterium target, vacuum vessels, four silicon double layers of the silicon vertex tracker and their support materials, the intermediate air volumes, and the solenoidal magnetic field. The CTof scintillation counter was not included in the simulation and not required for a successful proton detection.

Events of the reaction $D(e, e' p_S)X$ were generated and then the spectator protons tracked in the central detector, including energy loss due to ionization loss, multiple scattering in the materials, and accounting for the magnetic field effects. Detection in three of the four silicon double layers was required for a proton to be counted. This simulation part provided a flag whether the spectator proton was detected in the central tracker for every event. This information was included on an event-by-event basis as input for the FastMC, which tracked the scattered electron through the CLAS12 detector.

The results of this simulation for the proton momentum as a function of the scattering angle is shown in Fig. 12. The lowest spectator momentum detectable will be almost down to 200 MeV/$c$.

To be able to use the CToF for large backscattering angles, it would need to be extended in the upstream direction. In order to detect a proton scattered at the center of the 8 cm downstream shifted target cell at an angle of 160°, the CTof would need to be extended by 37.3 cm in the upstream direction, assuming its present radial position of 25.0 cm. We will study this and other possible modifications of the central tracker system to optimize the backward angle coverage.

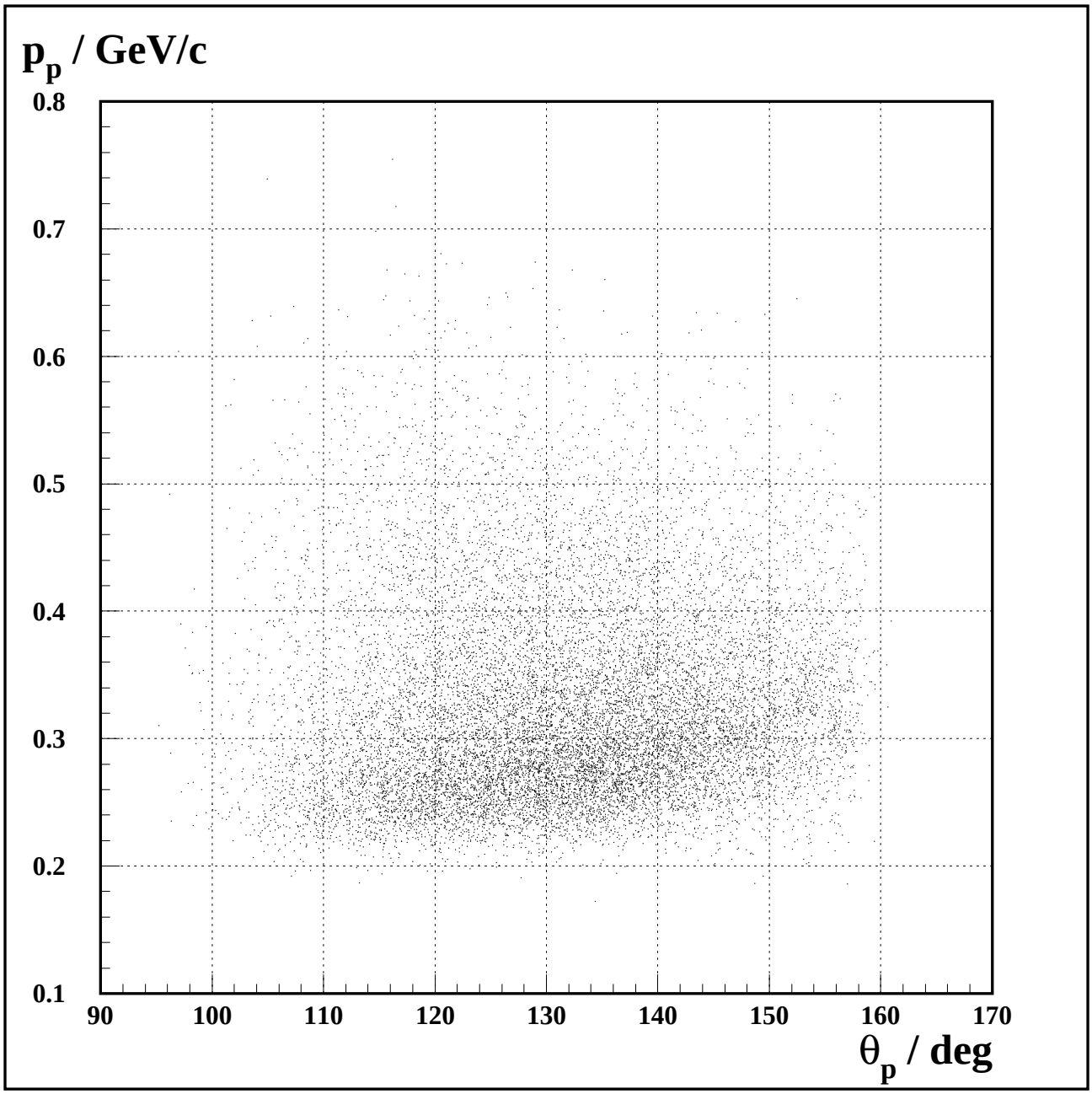


Figure 12: Simulation result for proton momentum as a function of scattering angle with a target central position moved downstream by 8 cm. Details in the text.

# 4 Expected Results

In the following, we discuss a few of the results we can extract from the data set collected under the conditions laid out in the previous section. Note that for a full proposal, we will have to work on optimizing the layout of the Central Tracker for this experiment, hopefully achieving better coverage at extreme backward proton angles. This should extend both the kinematic range and the statistical precision significantly above the preliminary results reported here.

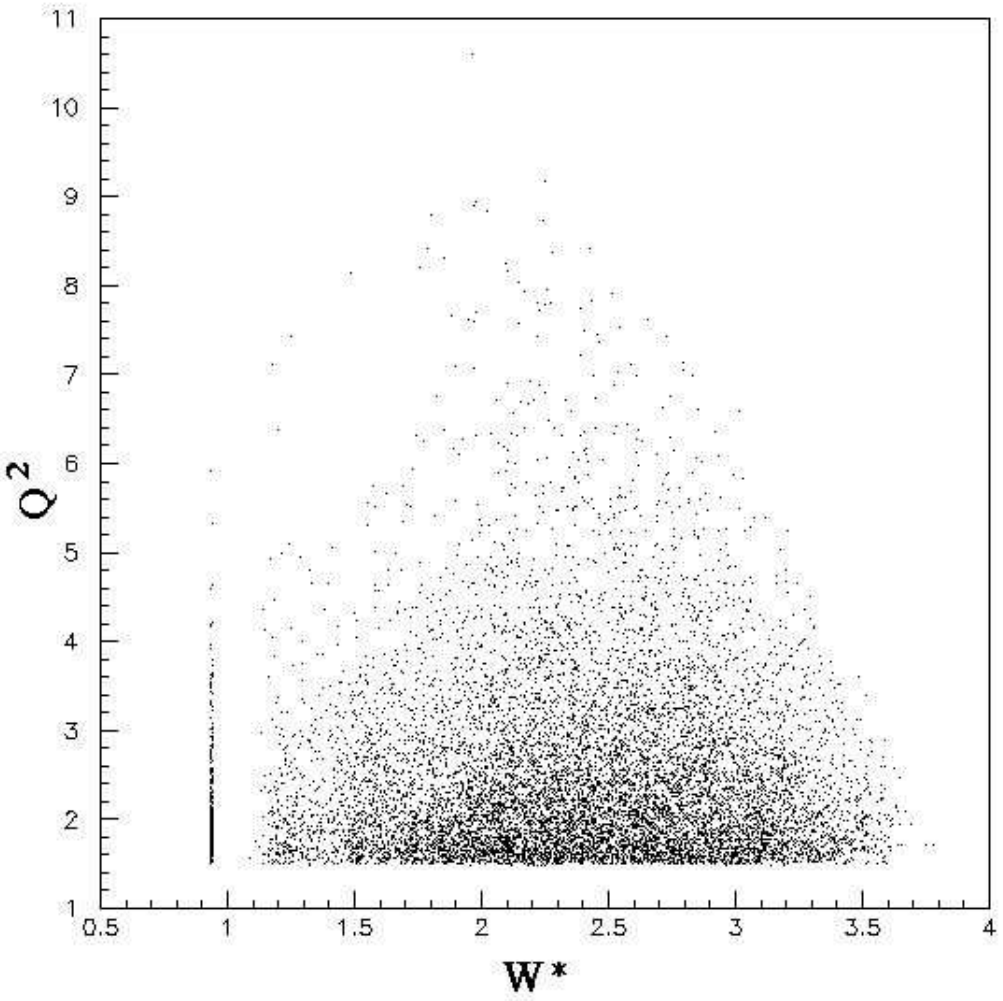


Figure 13: Kinematic coverage in final-state mass $W^*$ and $Q^2$ for 11 GeV beam.

As a first topic of interest, we look at the kinematic coverage in terms of the final-state mass $W^*$ and the momentum transfer range $Q^2$ reachable with 11 GeV beam (see Fig. 13). Clearly, we have good coverage of the elastic (pn final state), resonance and DIS region ($W^* > 2$ GeV), for relatively large momentum transfers $Q^2$. Of course, there are important physics topics to be addressed within the elastic and resonance region, for

instance, whether the resonance structure observed on free nucleons will survive with the same relative strength and at the same kinematic locations when the spectator proton is moving with high momentum. However, in the following we will concentrate only on DIS kinematics, where the interpretation can follow most closely the models discussed in the previous section.

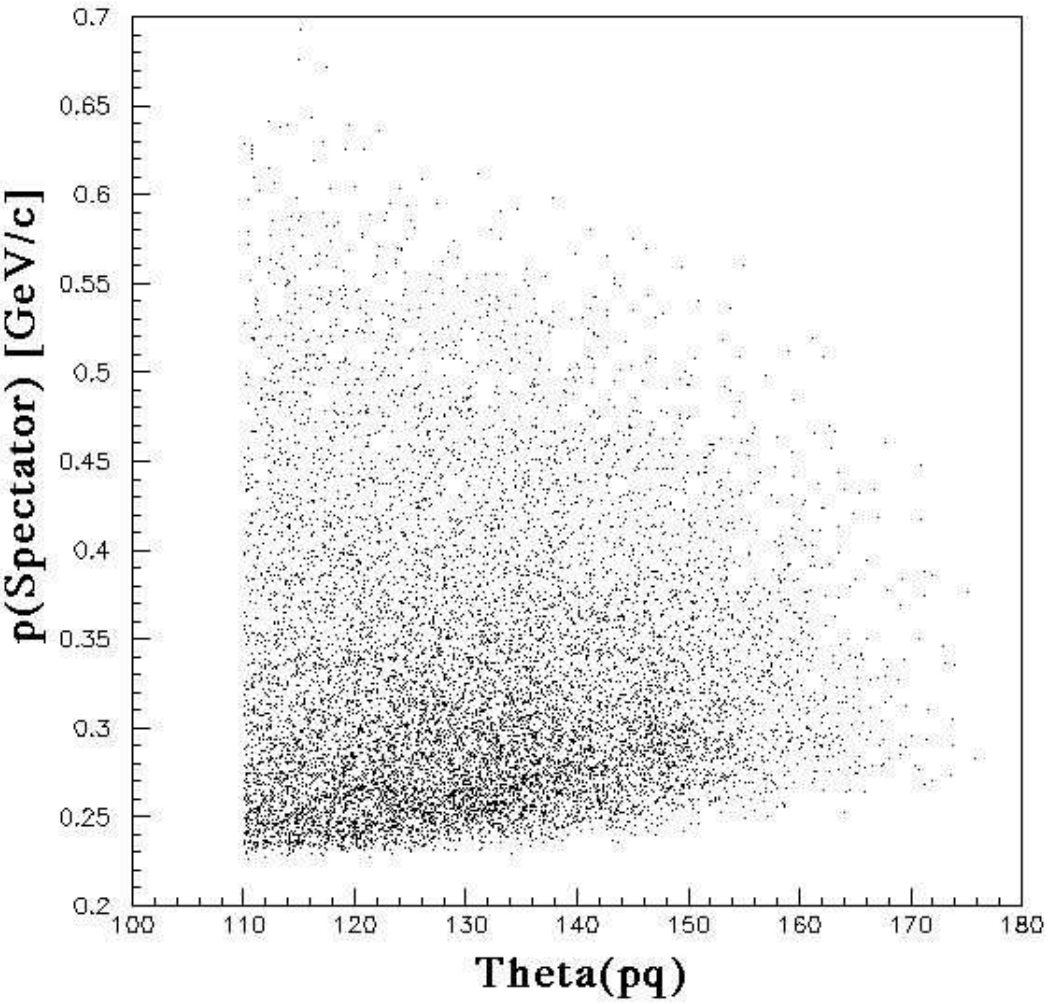


Figure 14: Coverage in the angle $\theta_{pq}$ between the direction of the momentum transfer $\mathbf{q}$ and the proton momentum, versus the magnitude of the proton momentum, for backwards-moving protons.

Our simulations show that we will collect a vast data set for kinematics where the spectator proton moves more or less sideways relative to the momentum transfer vector $\mathbf{q}$, with a detection threshold of momenta as low as 0.22 GeV/c and up to 0.7 GeV/c with excellent statistics. Overall, even if we restrict ourselves to DIS kinematics ($W^* > 2$ GeV and $Q^2 > 1.5$ GeV$^2$), we will cover the whole range in spectator light cone fraction, $0.8 < \alpha_s < 1.6$ down to transverse momenta of about 0.1 GeV/c. The minimum transverse momentum around $\alpha_s \approx 1$ is of course limited by our detection threshold, to be above 0.22 GeV/c. However,

the lower range of $p_T$ down to about 0.07 GeV/c and $0.9 < \alpha_s < 1.2$ will be filled in by the results from the BoNuS12 experiment. This will be an important "anchor point" for the comparison to various model predictions as shown in Fig. 7.

In the following, we will concentrate on the much more difficult to access kinematic region of large $\alpha_s$, which provides the most direct test of the various models for nucleon structure modifications within a tightly bound nucleon pair. In Fig. 14 we show the part of the Central Tracker acceptance above proton angles of 110 degree relative to $\mathbf{q}$, which contribute to these higher $\alpha_s$ values and, according to our results with E94-102, are less affected by FSI effects (see Fig. 1 in Section I). The most "valuable" kinematics is at large backward angles and moderate momentum (around 0.4 GeV/c), where we have coverage nearly to 170 degrees but low statistics.

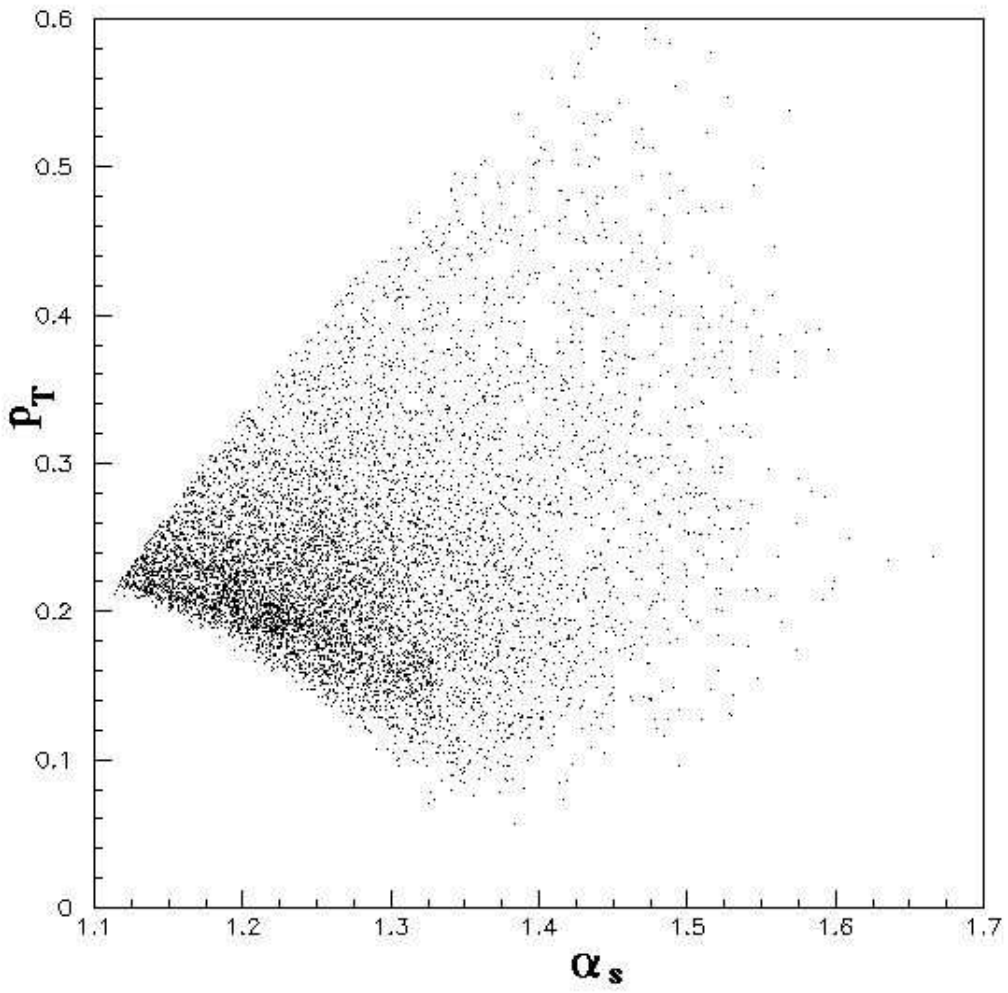


Figure 15: Equivalent coverage in the light cone variables $\alpha_s$ and $p_T$, only for events in the DIS region $W^* > 2$ GeV. Note that events at lower $\alpha_s$ and higher $p_T$ will be detected in copious amounts, but have been suppressed in this figure to emphasize larger backward angles, $\theta_{pq} > 110°$.

The next figure 15 shows the corresponding coverage in the $\alpha_s, p_T$ plane. This figure

shows a reasonably good coverage down to $p_T \approx 0.1$ GeV/c for $\alpha_s$ well exceeding 1.4. The coverage in $\alpha_s$ is of course correlated with that in the kinematically scaled Bjorken variable $x^*$, as shown in Fig. 16 . This figure indicates that we indeed cover a range in $\alpha_s$ of at least 1 – 1.4 simultaneously with a range in $x^*$ of 0.2 – 0.6, all within the DIS region, which is required for the comparison to models as in Fig. 7.

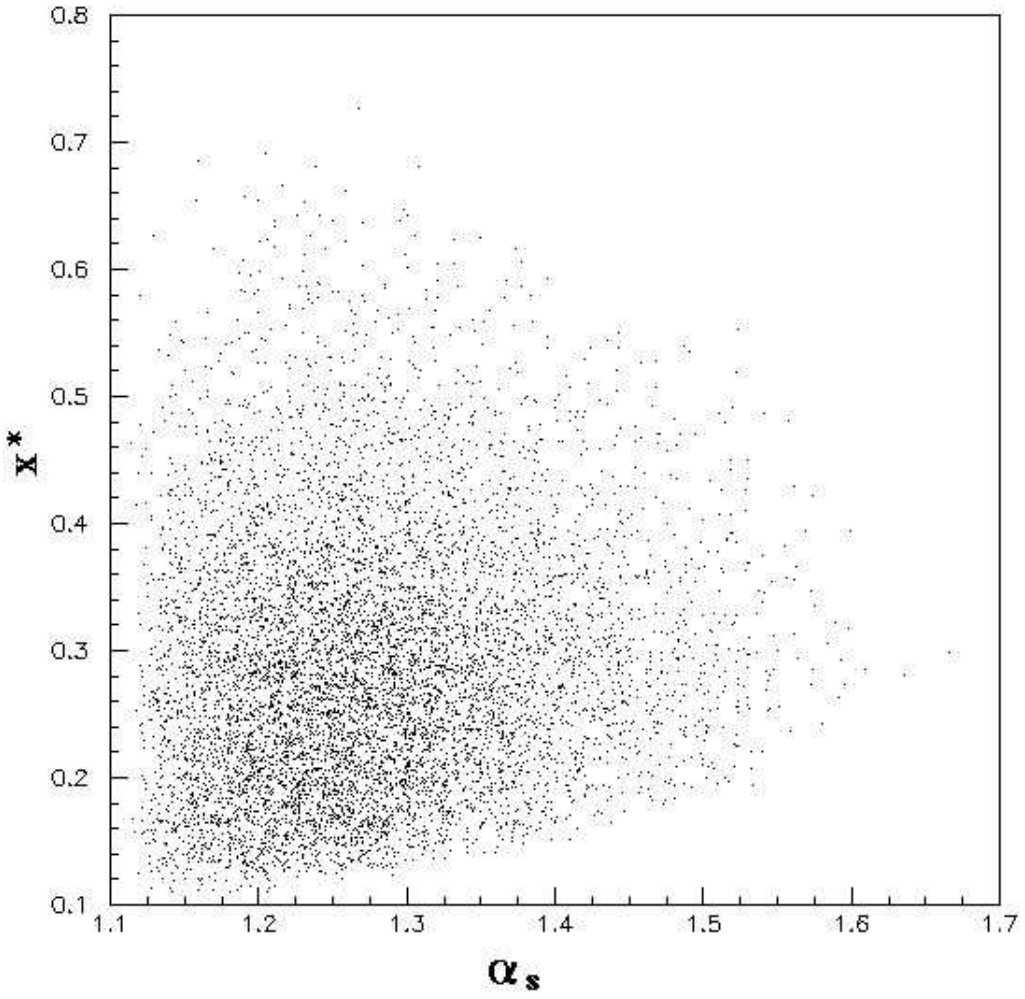


Figure 16: Distribution of expected DIS events over the variables $\alpha_s$ and $x^*$.

Our final plot Fig. 17 shows the expected number of counts in the "hardest to access corner" of the 4-dimensional kinematic "phase space" - large $\alpha_s > 1.3$, small $p_T < 0.2$ GeV/c, and large $x^*$ (within the DIS region). Under these conditions, we will have data up to $\alpha_s \approx 1.5$ covering the whole $x^*$–range needed for the comparison. The count rate will be rather low for the most extreme kinematics (a total of about 30 counts each in both the highest two $\alpha_s$ bins and for the highest bins in $x^*$ of width 0.01). One can improve the statistics by combining 2 or more bins in $x^*$, since our resolution will anyway be somewhat worse than 0.01 in that kinematic region. We will get two data points with relative errors of about 10-15% statistical error at the high–$\alpha_s$ range of Fig. 7, enough to make statistically

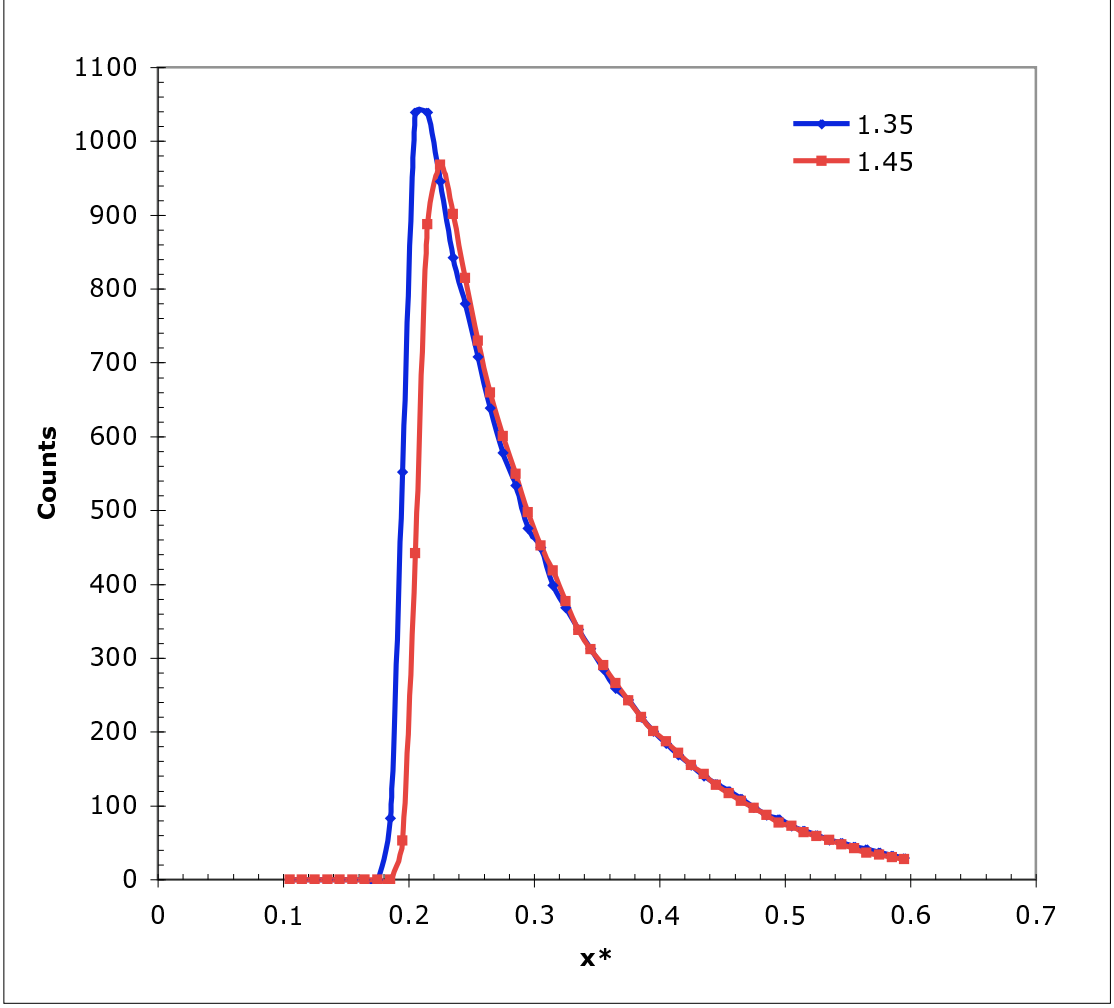


Figure 17: Expected number of counts for the highest two bins of spectator light cone fraction $\alpha_s$ (with central values of $\alpha_s = 1.35$ and $\alpha_s = 1.45$), for 30 days of running with CLAS12 and standard luminosity on deuterium. Only events in the DIS region ($W^* > 2$) and with low $p_T < 0.2$ GeV/c are included. At the highest $x^* = 0.6$, we expect about 25 counts per bin of $\Delta\alpha_s = 0.1$ and $\Delta x^* = 0.01$, allowing us to determine the ratio $F_2^{n(eff)}(x^* = 0.6)/F_2^{n(eff)}(x^* = 0.2)$ with an uncertainty of better than 20%. The statistical error can be improved by combining 2 or more of our rather narrow $x^*$ bins. Requiring $p_T < 0.15$ would increase the statistical errors by a factor of 2.4 unless we modify the central tracker to increase backward angle acceptance.

significant distinctions between the various models shown there. For the full proposal, we will add a careful analysis of systematic errors, but expect those to be significantly smaller in size. A careful analysis of possible modifications of the Central Tracker may well point the way to a significant increase in coverage for this crucial kinematic region, with correspondingly reduced errors.

# 5 Summary

Our studies have shown that we can extract the dependence of the structure function $F_{2n}^{(eff)}(x^*, Q^2, \alpha_s, p_T)$ at fixed $x^*$ between 0.2 and 0.6 and fixed $p_T < 0.2$ GeV/c on the

spectator light cone fraction $\alpha_s$ over the full range of interest, $1 \leq \alpha_s \leq 1.4$, by combining the results of BoNuS12 with the measurements proposed here. We will cover a large range in $x^*$ and $Q^2$, allowing us to make detailed comparisons with different models described in this LOI.

We believe that this goal can be achieved with a rather modest modification of the standard target and detector configuration of CLAS12. However, we consider it advantageous to look into several options (using deposited charge in the SVT for proton PID, building a dedicated ToF array covering the most backward angles, rearranging the SVT relative to the target to optimize back angle coverage) before developing a full proposal. We expect to submit such a proposal within 1-2 years.

# References


[1] C.E. Carlson, K.E. Lassila and U.P. Sukhatme, Phys. Lett. **B 263**, 377 (1991); C.E. Carlson and K.E. Lassila, Phys. Rev. C **51**, 364 (1995).

[2] W. Melnitchouk and A.W. Thomas, Phys. Lett. **B377**, 11 (1996); W. Melnitchouk, A.W. Schreiber and A.W. Thomas, Phys. Rev. D **49**, 1183 (1994).

[3] F.E. Close, R.L. Jaffe, R.G. Roberts, and G.G. Ross, Phys. Rev. D **31**, 1004 (1985);

[4] L.L. Frankfurt and M.I. Strikman, Phys. Rep. **76**, 217 (1981).

[5] L.L. Frankfurt and M.I. Strikman, Nucl. Phys. **B250**, 1585 (1985); Phys. Rep. **160**, 235 (1988).

[6] M.M. Sargsian *et al.*, J. Phys. G **29**, R1 (2003).

[7] J.J. Aubert *et al.*, Phys. Lett. **B123**, 275 (1983).

[8] S.A. Kulagin and R. Petti, Nucl. Phys. **A765**, 126 (2006).

[9] C.E. Carlson, J.Hanlon, and K.E. Lassila, Phys. Rev. D **63**, 117301 (2001);

[10] T. Kafka *et al.*, Bull. Am. Phys. Soc. **28**, 756 (1983).

[11] E. Matsinos *et al.*, Zeitschr. f. Phys. C **44**, 79 (1989).

[12] A.V. Klimenko, S.E. Kuhn, *et al.*, Phys. Rev. C **73**, 035212 (2006).

[13] S. Bültmann *et al.*, Proposal PR12-06-113, conditionally approved by PAC30.

[14] C. Ciofi degli Atti and B.Z. Kopeliovich, Eur. Phys. J. A **17**, 133 (2003); C. Ciofi degli Atti, L.P. Kaptari and B.Z. Kopeliovich, Eur. Phys. J. A **19**, 145 (2004).

[15] W. Melnitchouk, M. Sargsian and M.I. Strikman, Z. Phys. **A359**, 99 (1997).

[16] See e.g. R.P. Bickerstaff and A.W. Thomas, J. Phys. G **15**, 1523 (1989).

[17] W. Melnitchouk, A.W. Schreiber and A.W. Thomas, Phys. Lett. **B335**, 11 (1994); Phys. Rev. D **49**, 1183 (1994).

[18] C. Ciofi degli Atti and S. Simula, Phys. Lett. **B319**, 23 (1993); Few-Body Systems **18**, 55 (1995); S. Simula, Phys. Lett. **B387**, 245 (1996); Few-Body Systems Suppl. **9**, 466 (1995).

[19] G.D. Bosveld, A.E.L. Dieperink and A.G. Tenner, Phys. Rev. C **49**, 2379 (1994).

[20] F. Gross and S. Liuti, Phys. Rev. C **45**, 1374 (1992); S. Liuti and F. Gross, Phys. Lett. **B356**, 157 (1995).

[21] S.A. Kulagin, G. Piller and W. Weise, Phys. Rev. C **50**, 1154 (1994); S.A. Kulagin, W. Melnitchouk, G. Piller and W. Weise, Phys. Rev. C **52**, 932 (1995).

[22] S.I. Alekhin, S.A. Kulagin and S. Liuti, Phys. Rev. D **69**, 114009 (2004).

[23] L. Heller and A.W. Thomas, Phys. Rev. C **41**, 2756 (1990).

[24] L.L. Frankfurt *et al.*, Z. Phys. **A352**, 97 (1995); Phys. Lett. **B369**, 201 (1996).

[25] M.I. Strikman, M. Tverskoy and M. Zhalov, nucl-th/9609055, *Proceedings of Workshop "Future Physics at HERA"*, Hamburg, 1085 (1996).

[26] M.R. Adams *et al.*, Phys. Rev. Lett. **74**, 5198 (1995).

[27] B.Z. Kopeliovich, J. Nemchik and E. Predazzi, hep-ph/9511214, *Proceedings of the ELFE Summer School on Confinement Physics*, ed. S.D. Bass and P.A.M. Guichon, Editions Frontieres, Gif-sur-Yvette, 391 (1995).

[28] C. Ciofi degli Atti, L.P. Kaptari and D. Treleani, Phys. Rev. C **63**, 044601 (2001).

[29] C. Ciofi degli Atti, L.P. Kaptari and B.Z. Kopeliovich, Eur. Phys. J. A **19**, 145 (2004).